Reduction of Momentum and Spin Relaxation Rate in Strained Thin Silicon Films

D. Osintsev, V. Sverdlov, and S. Selberherr
Institute for Microelectronics, TU Wien, Gußhausstraße 27–29 / E360, Wien, Austria
E-mail: {Osintsev|Sverdlov|Selberherr}@iue.tuwien.ac.at

***Abstract*—We investigate the surface roughness and phonon induced spin and momentum relaxation in ultra-scaled SOI MOSFETs. We show that the spin-flip hot spots characterized by strong spin relaxation can be efficiently removed by applying shear strain resulting in an increase of spin lifetime by orders of magnitude. In contrast, the momentum relaxation time in ultrathin films, which is mostly determined by surface roughness scattering can be only increased by a factor of two, in agreement with strain-induced mobility enhancement data.**

I. INTRODUCTION

Future microelectronic devices should substantially reduce the power consumption per operation. In addition, novel devices have to be smaller and faster. Spintronics considers novel devices which use the spin of electrons instead of the charge to perform an operation. A number of devices has already been proposed [1,2]. Silicon is an ideal material for spintronic devices [3], because it is composed of nuclei with predominantly zero spin and is characterized by small spin-orbit coupling. Both factors favour to reduce the spin relaxation. However, the experimentally observed enhancement of spin relaxation in electrically gated lateral-channel silicon structures [4] could compromise the reliability and become an obstacle in realizing spin-driven devices. Thus, deeper understanding of spin relaxation mechanisms in thin silicon films is urgently needed [5].

II. MODEL

We present an approach to analyze surface roughness and phonon induced spin relaxation in thin silicon films. We investigate the dependences on temperature and uniaxial [110] shear strain for different (001)-oriented silicon films. We are considering three mechanisms which contribute to the spin and momentum relaxation: surface roughness (SR), intra- and intervalley (for spin relaxation) scattering by acoustic phonons. The intrasubband and intersubband surface roughness scattering matrix elements are taken proportional to the square of the product of the subband function derivatives at the interface [6]. The spin and momentum relaxation times are calculated by thermal averaging [5-7] as:

$$\frac{1}{\tau}=\frac{\int\frac{1}{\tau(\mathbf{K_1})}f(\varepsilon)\left(1-f(\varepsilon)\right)d\mathbf{K_1}}{\int f(\varepsilon)\,d\mathbf{K_1}}, \qquad (1)$$

$$\int d\mathbf{K_1}=\int_0^{2\pi}\int_0^{\infty}\frac{|\mathbf{K_1}|}{\left|\frac{\partial\varepsilon(\mathbf{K_1})}{\partial\mathbf{K_1}}\right|}d\varphi\, d\varepsilon. \qquad (2)$$

The surface roughness spin relaxation rate is calculated in the following way:

$$\frac{1}{\tau_{SR}(\mathbf{K_1})}=\frac{4\pi}{\hbar(2\pi)^2}\sum_{i,j=1,2}\int_0^{2\pi}\pi\Delta^2L^2\frac{1}{\epsilon_{ij}^2(\mathbf{K_2}-\mathbf{K_1})}\frac{\hbar^4}{4m_l^2}\frac{|\mathbf{K_2}|}{\left|\frac{\partial\varepsilon(\mathbf{K_2})}{\partial\mathbf{K_2}}\right|}\cdot$$
$$\cdot\left[\left(\frac{d\Psi_{i\mathbf{K_1}\sigma}}{dz}\right)^*\frac{d\Psi_{j\mathbf{K_2}-\sigma}}{dz}\right]^2_{z=\pm\frac{t}{2}}\exp\left(\frac{-(\mathbf{K_2}-\mathbf{K_1})^2L^2}{4}\right)d\varphi, \qquad (3)$$

where ε is the electron energy, $\mathbf{K_{1,2}}$ are the in-plane wave vectors before and after scattering, ϵ_{ij} is the dielectric permittivity, L is the autocorrelation length, Δ is the mean square value of the surface roughness fluctuations, $\Psi_{i\mathbf{K_1}}$ and $\Psi_{j\mathbf{K_2}}$ are the wave functions, $f(\varepsilon)$ is the Fermi function, and σ is the spin projection to the [001] axis.

The momentum relaxation time is evaluated in the standard way [6]. The spin relaxation rate due to the transversal acoustic phonons is calculated as:

$$\frac{1}{\tau_{TA}(\mathbf{K_1})}=\frac{2\pi k_BT}{\hbar\rho v_{TA}^2}\sum\int_0^{2\pi}\frac{|\mathbf{K_2}|}{\left|\frac{\partial\varepsilon(\mathbf{K_2})}{\partial\mathbf{K_2}}\right|}\cdot$$
$$\cdot\left[1-\frac{\frac{\partial\varepsilon(\mathbf{K_2})}{\partial\mathbf{K_2}}f(\varepsilon(\mathbf{K_2}))}{\frac{\partial\varepsilon(\mathbf{K_1})}{\partial\mathbf{K_1}}f(\varepsilon(\mathbf{K_1}))}\right]\frac{1}{2}\int_0^t\int_0^t\exp\left(-\sqrt{q_x^2+q_y^2}|z-z'|\right)\cdot$$
$$\cdot\left[\Psi_{\mathbf{K_2}}^\dagger(z)M\Psi_{\mathbf{K_1}}(z)\right]\left[\Psi_{\mathbf{K_2}}^\dagger(z')M\Psi_{\mathbf{K_1}}(z')\right]\cdot$$
$$\cdot\left[\sqrt{q_x^2+q_y^2}-\frac{8q_x^2q_y^2-\left(q_x^2+q_y^2\right)^2}{q_x^2+q_y^2}|z-z'|\right]dzdz', \qquad (4)$$

with k_B is the Boltzmann constant, T is the temperature, $\rho=2329\frac{\mathrm{kg}}{\mathrm{m}^3}$ is the silicon density, $v_{TA}=5300\frac{\mathrm{m}}{\mathrm{s}}$ is the transversal phonons velocity, t is the film thickness, $\left(q_x,q_y\right)=\mathbf{K_1}-\mathbf{K_2}$, and M is the matrix 4×4. Written in the basis for the spin relaxation rate the matrix M is:

$$M=\begin{bmatrix}0 & 0 & \frac{D_{xy}}{2} & 0\\ 0 & 0 & 0 & \frac{D_{xy}}{2}\\ \frac{D_{xy}}{2} & 0 & 0 & 0\\ 0 & \frac{D_{xy}}{2} & 0 & 0\end{bmatrix}. \qquad (5)$$

Here D_{xy}=14eV is the shear deformation potential.

This work is supported by the European Research Council through the grant #247056 MOSILSPIN.

The intravalley spin relaxation rate due to the longitudinal acoustic phonons is calculated as:

$$\frac{1}{\tau_{LA}(\mathbf{K_1})} = \frac{2\pi k_B T}{\hbar\rho v_{LA}^2}\sum\int_0^{2\pi}\frac{|\mathbf{K_2}|}{\left|\frac{\partial\varepsilon(\mathbf{K_2})}{\partial\mathbf{K_2}}\right|}\cdot$$
$$\cdot\left[1-\frac{\frac{\partial\varepsilon(\mathbf{K_2})}{\partial\mathbf{K_2}}f(\varepsilon(\mathbf{K_2}))}{\frac{\partial\varepsilon(\mathbf{K_1})}{\partial\mathbf{K_1}}f(\varepsilon(\mathbf{K_1}))}\right]\frac{1}{2}\int_0^t\int_0^t\exp\left(-\sqrt{q_x^2+q_y^2}|z-z'|\right)\cdot$$
$$\cdot\left[\Psi_{\mathbf{K_2}}^{\dagger}(z)M\Psi_{\mathbf{K_1}}(z)\right]\left[\Psi_{\mathbf{K_2}}^{\dagger}(z')M\Psi_{\mathbf{K_1}}(z')\right]\cdot$$
$$\cdot\frac{4q_x^2q_y^2}{\left(\sqrt{q_x^2+q_y^2}\right)^3}\left[\sqrt{q_x^2+q_y^2}|z-z'|+1\right]dzdz'. \quad (6)$$

Here v_{LA}=8700$\frac{\mathrm{m}}{\mathrm{s}}$ is the speed of the longitudinal phonons and the matrix M is defined with (5).

The intervalley spin relaxation rate contains the Elliot and Yafet contributions [5], which are calculated in the following way:

$$\frac{1}{\tau_{LA}(\mathbf{K_1})} = \frac{2\pi k_B T}{\hbar\rho v_{LA}^2}\sum\int_0^{2\pi}\frac{|\mathbf{K_2}|}{\left|\frac{\partial\varepsilon(\mathbf{K_2})}{\partial\mathbf{K_2}}\right|}\left[1-\frac{\frac{\partial\varepsilon(\mathbf{K_2})}{\partial\mathbf{K_2}}f(\varepsilon(\mathbf{K_2}))}{\frac{\partial\varepsilon(\mathbf{K_1})}{\partial\mathbf{K_1}}f(\varepsilon(\mathbf{K_1}))}\right]\cdot$$
$$\cdot\frac{1}{2}\int_0^t\left[\Psi_{\mathbf{K_2}}^{\dagger}(z)M\Psi_{\mathbf{K_1}}(z)\right]^*\left[\Psi_{\mathbf{K_2}}^{\dagger}(z)M\Psi_{\mathbf{K_1}}(z)\right]dz. \quad (7)$$

Here the matrix M is written as:

$$M = \begin{bmatrix} M_{ZZ} & M_{SO} \\ M_{SO}^{\dagger} & M_{ZZ} \end{bmatrix}, \quad (8)$$

$$M_{ZZ} = \begin{bmatrix} D_{ZZ} & 0 \\ 0 & D_{ZZ} \end{bmatrix}, \quad (9)$$

$$M_{SO} = \begin{bmatrix} 0 & D_{SO}(q_y - iq_x) \\ D_{SO}(-q_y - iq_x) & 0 \end{bmatrix}, \quad (10)$$

D_{ZZ}=12eV, D_{SO}=15meV/k$_0$ with $k_0 = 0.15\times 2\pi/a$ defined as the position of the valley minimum relative to the *X*-point in unstrained silicon [5].

In order to find the subband wave functions and subband energies a perturbative **k·p** approach [7-9] suitable to describe the electron subband structure in the presence of strain and spin-orbit interaction is applied. We consider only the two relevant valleys along the [001] axis. The Hamiltonian is written in the vicinity of the *X*-point along the k_z-axis in the Brillouin zone [10]. In order to find the subband wave functions and subband energies the Hamiltonian [10] is transformed to eliminate the coupling between the spins with opposite direction in different valleys.

$$H = \begin{bmatrix} H_1 & H_3 \\ H_3 & H_2 \end{bmatrix}, \quad (11)$$

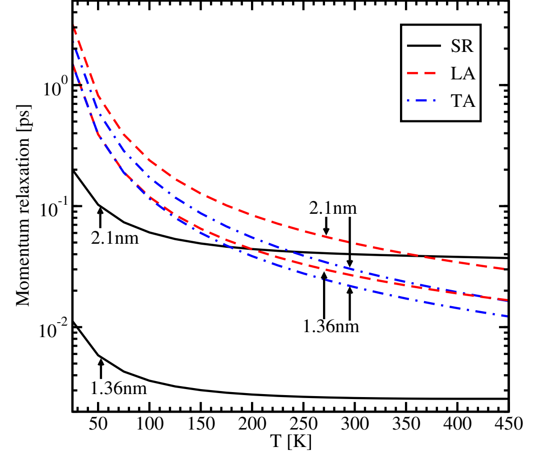

Figure 1. Dependence of the momentum relaxation time induced by surface roughness(SR), longitudinal phonons (LA), and transversal phonons (TA) on temperature for two different thicknesses, ε_{xy}=0, and electron concentration 1.29·10^{12}cm^{-2}

H_1, H_2, and H_3 are written as:

$$H_{1,2} = \left[\frac{\hbar^2 k_z^2}{2m_l} + \frac{\hbar^2(k_x^2+k_y^2)}{2m_t} + (-1)^j\delta\right]I, \quad (12)$$

$$H_3 = \begin{bmatrix} \frac{\hbar^2 k_0 k_z}{m_l} & 0 \\ 0 & \frac{\hbar^2 k_0 k_z}{m_l} \end{bmatrix}. \quad (13)$$

Here $\delta = \sqrt{\left(D\varepsilon_{xy} - \frac{\hbar^2 k_x k_y}{M}\right)^2 + \Delta_{SO}^2\left(k_x^2+k_y^2\right)}$, I is the identity 2×2 matrix, m_t and m_l are the transversal and the longitudinal silicon effective masses, $M^{-1}\approx m_t^{-1} - m_0^{-1}$, ε_{xy} denotes the shear strain component, and D = 14eV is the shear strain deformation potential, Δ_{SO}=1.27meVnm is the effective spin-orbit interaction [10]. Then the approach similar to that used for the two-band **k·p** Hamiltonian written in the vicinity of the *X*-point of the Brillouin zone for silicon films under uniaxial strain [7] is applicable to find the subband functions and subband energies.

III. RESULT AND DISCUSSION

Figure 1 shows the dependence of the momentum relaxation time on temperature. The contributions from the surface roughness (SR), the longitudinal acoustic phonons (LA), and the transversal acoustic phonons are shown. For the film thicknesses 2.1nm and 1.36nm the contribution from the surface roughness is dominant at low temperatures. However, for a temperature around 240K the contribution from the surface roughness and from the acoustic phonons for the film of thickness 2.1nm are equal. Any further increase of temperature leads to higher values of the momentum relaxation time caused by acoustic phonons. Figure 1 shows that the dominant relaxation mechanism strongly depends on film thickness. The phonons limited momentum relaxation is

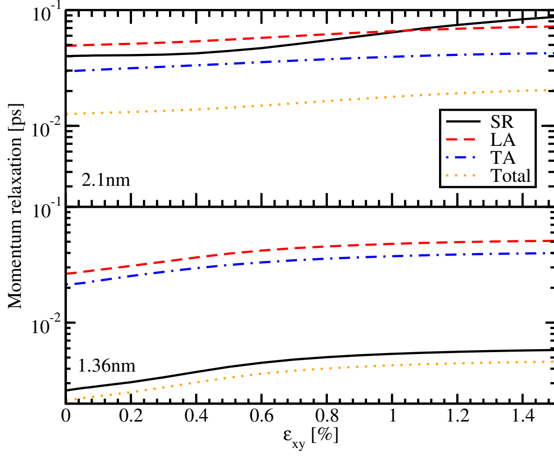

Figure 2. Dependence of the momentum relaxation time induced by surface roughness(SR), longitudinal phonons (LA), and transversal phonons (TA) on shear strain for 1.36nm and 2.1nm film thickness, for T=300K, and electron concentration $1.29{\cdot}10^{12}$cm^{-2}

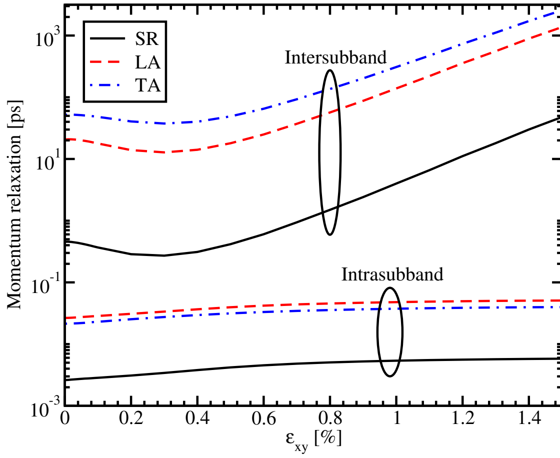

Figure 3. Dependence of the intersubband and intrasubband components of the momentum relaxation time induced by surface roughness(SR), longitudinal phonons (LA), and transversal phonons (TA) on shear strain for the film thickness 1.36nm, T=300K, and electron concentration $1.29{\cdot}10^{12}$cm^{-2}

characterized by a much weaker thickness dependence and does not change significantly while the thickness decreases from 2.1nm to 1.36nm. The surface roughness limited momentum relaxation decreases by more than an order of magnitude because of the expected t^6 dependence [6,11]. Thus, for the thickness 1.36nm the surface roughness induced spin relaxation is the dominant mechanism for the whole range of considered temperatures.

Figure 2 shows the dependence of the different mechanisms of the momentum relaxation together with the total momentum relaxation time on shear strain. The improvement of the momentum relaxation time due to the shear strain is around 60% for the film thickness of 2.1nm and around 110% for the film thickness 1.36nm. The transversal acoustic phonons limited momentum relaxation improves around 45% for 2.1nm and for

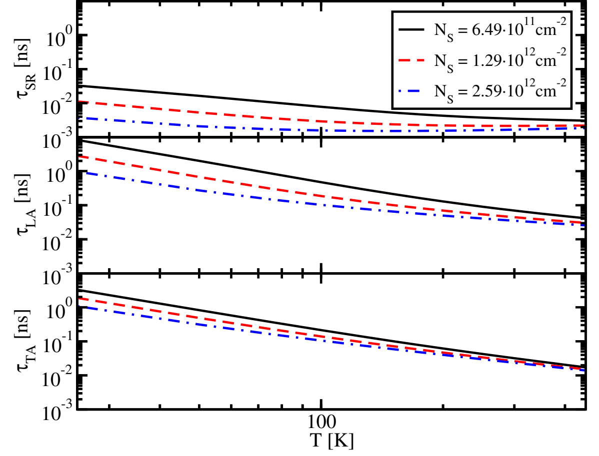

Figure 4. Dependence of the surface roughness (SR), the longitudinal phonons' (LA), and the transversal phonons' (TA) contribution to the spin lifetime on temperature for different values of the electron concentration, for ε_{XY}=0, and film thickness 2.1nm

1.36nm. The surface roughness limited momentum relaxation time increases around 120% for 2.1nm and for 1.36nm. Because the SR mechanism is the dominant for the film thickness 1.36nm, the increase of the total momentum relaxation time is higher for 1.36nm than for 2.1nm. We point out that the increase of the momentum relaxation time is due to the corresponding scattering matrix elements dependences on strain. Combined with the strain induced transport effective mass decrease it should result in an even better mobility improvement supporting the use of uniaxial tensile strain as the mobility booster in fully depleted ultra-thin SOI FETs.

Figure 3 demonstrates the contribution of the inter- and intrasubband processes to the LA, TA, and SR limited momentum relaxation. The domination of the intrasubband relaxation processes for all three mechanisms of the momentum relaxation is shown, in agreement with the selection rule that the elastic processes result in strong intrasubband relaxation. The LA and TA mechanisms should be considered, since their intrasubband contributions are of the same order. The domination of the SR mechanism for the film thickness 1.36nm shown in Figure 1 and Figure 2 is the consequence of the high intrasubband relaxation rate.

The dependence of the spin lifetime on temperature for phonon scattering, and SR scattering for different carrier concentrations is shown in Figure 4. The spin relaxation is more efficient for higher carrier concentrations for all three considered mechanisms. While the temperature increases, the difference between the spin lifetimes for different values of the electron concentration becomes less pronounced. Figure 4 shows that the SR mechanism dominates for all concentration values. Relaxation because of the LA phonons induced intravalley scattering shows the largest spin lifetime among the three considered mechanisms.

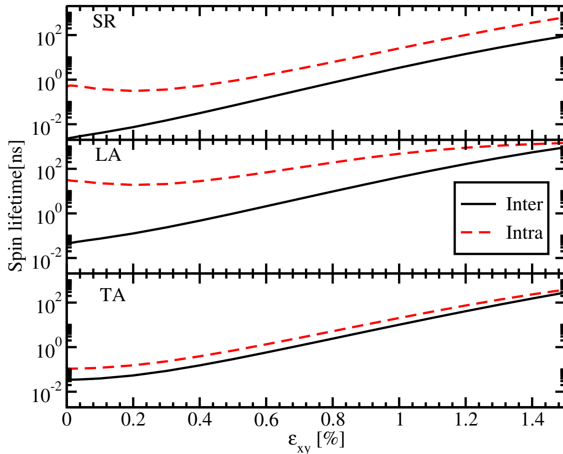

Figure 5. Dependence of the intersubband and the intrasubband component of the spin lifetime for different spin relaxation mechanisms (surface roughness(SR), longitudinal phonons (LA), and transversal phonons (TA)) on shear strain for the film thickness 1.36nm, T=300K, and electron concentration $1.29{\cdot}10^{12}\text{cm}^{-2}$

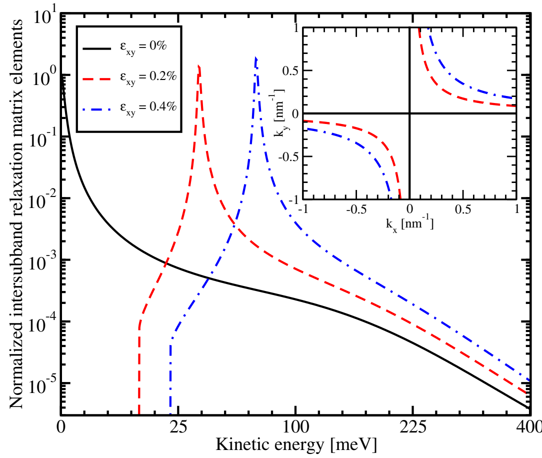

Figure 6. Normalized intersubband relaxation matrix elements as a function of the conduction electrons kinetic energy in [110] direction. The inset shows the positions of the hot spots for different values of shear strain.

Figure 5 demonstrates that the main contribution to the spin lifetime comes from the intersubband processes. This is due to the presence of the spin relaxation hot spots characterized by the sharp peaks of the intersubband spin relaxation matrix elements. Their position is shown in Figure 6. For higher shear strain values the hot spots are pushed to higher energies away from the subband minima (inset in Figure 6). The strong increase of the spin lifetime on shear strain for SR and the phonon mechanisms is shown in Figure 7. SR remains the dominant mechanism determining spin relaxation in thin silicon films.

IV. Conclusion

We have investigated thin silicon films by utilizing a generalized **k·p** Hamiltonian which includes the spin-orbit contribution for the momentum and the spin relaxation time in thin silicon films

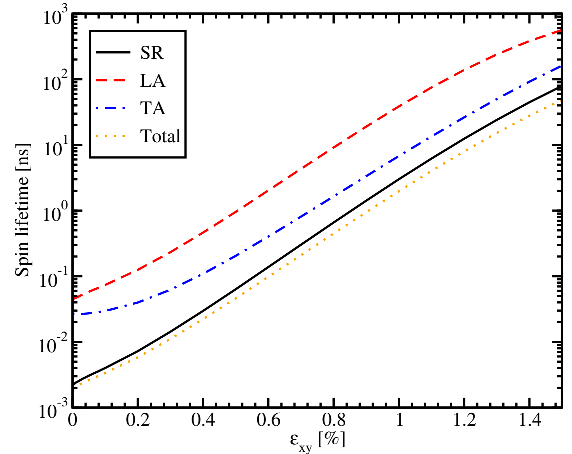

Figure 7. Dependence of the spin lifetime on shear strain for the film thickness 1.36nm, T=300K,and electron concentration $1.29{\cdot}10^{12}\text{cm}^{-2}$

for different thicknesses, shear strain values, and temperatures. We have shown that the momentum relaxation time for 1.36nm wide silicon film is determined by surface roughness scattering and can be increased by 110%, while applying shear tensile strain, in contrast to the 2.1nm thin film, where it can only be boosted by 60% due to the strong contribution of phonons. We have demonstrated a strong, several orders of magnitude, increase of spin lifetime in strained silicon films. Thus shear strain used to boost mobility can also be used to increase spin lifetime.

Acknowledgment

The computational results have been achieved in part using the Vienna Scientific Cluster (VSC).

References

[1] S. Sugahara and J. Nitta,"Spin transistor electronics: An overview and outlook", Proceedings of the IEEE, **98**(12), 2124–2154 (2010).

[2] S. Datta and B. Das,"Electronic analog of the electro-optic modulator", Appl. Phys. Lett., **56**, 665 (1990).

[3] R. Jansen, "Silicon spintronics", Nat.Mater., **11**, 400–408 (2012).

[4] L.Li, I.Appelbaum, "Modeling spin transport in electrostatically-gated lateral-channel silicon devices: Role of interfacioal spin relaxation", Phys Rev.B., **84**, 165318 (2011).

[5] Y. Song, H. Dery, "Analysis of phonon-induced spin relaxation processes in silicon", Phys. Rev. B, **86**, 085201 (2012).

[6] M. V. Fischetti et al., "Six-band k·p calculation of hole mobility in silicon inversion layers: Dependence on surface orientation, strain, and silicon thickness", J.App.Phys., **94**, 1079 (2003).

[7] P. Li, H. Dery, "Spin-orbit symmetries of conduction electrons in silicon", Phys. Rev. Lett., **107**, 107203 (2011).

[8] G.L. Bir, G.E. Pikus, *Symmetry and strain-induced effects in semiconductors.* New York/Toronto: J. Wiley & Sons 1974.

[9] V. Sverdlov, *Strain-induced effects in advanced MOSFETs.* Wien - New York. Springer 2011.

[10] D. Osintsev et al., "Reduction of serface roughness induced spin relaxation in soi structures: an analytical approach", Proc. EUROSOI (2013).

[11] S. Jin, M.V. Fischetti, T.-W. Tang, "Modeling of surface roughness scattering in ultrathin-body SOI MOSFETs", IEEE Trans. Electron Devices **54**(9), 2191–2202 (2007).